Electronic Transactions on Numerical Analysis.
Volume 59, pp. 250–269, 2023.

ISSN 1068–9613.
DOI: 10.1553/etna_vol59s250

ETNA
Kent State University and
Johann Radon Institute (RICAM)

COMPUTATION OF POTENTIAL FLOW IN MULTIPLY CONNECTED DOMAINS USING CONFORMAL MAPPING*

T. DELILLO†, J. MEARS†, AND S. SAHRAEI‡

Dedicated to Lothar Reichel on the occasion of his 70th birthday.

Abstract. This paper describes a method to calculate the potential flow in domains in the complex plane exterior to a finite number of closed curves using conformal mapping. A series method is used to compute the potential flow over multiply connected circle domains. The flow is then mapped from the circle domain to the target physical domain by a method which approximates the Laurent series of the conformal map. The circulations around each boundary can be specified. For flow over multi-element airfoils, the circulations are computed to satisfy the Kutta condition at the trailing edges. The linear systems which are solved on the circle domain for both the potential flow and the conformal maps are of the form identity plus a low-rank matrix, allowing for the efficient use of conjugate-gradient-like methods.

Key words. Potential flow, numerical conformal mapping, multiply connected domains, series methods, airfoils, Kutta condition.

AMS subject classifications. 30C30, 65E05

1. Introduction.

We compute the potential flow over multiply connected domains using conformal mapping methods [5, 10] for mapping the exterior of m nonoverlapping disks to the exterior of m given curves with smooth boundaries. The potential flow is computed in the circle domain using a series method developed in [9]. The complex velocity potential is analytic and transplants under conformal mapping. The flow is uniform at infinity with specified circulations around the boundaries.

Similar calculations were performed in [11] for flow over multi-element airfoils using a less efficient reflection method to compute the flows. The method requires reflections of circles in circles and converges slowly, if at all, as the connectivity m increases. Another more efficient approach uses the Schottky-Klein prime function [7] to compute the flow in the circle domain. The prime function was recently combined in [8] with the conformal mapping method [5] to compute flow over multi-element airfoils, such as those considered here. In [8], comparisons were made to a modified version of the series method discussed here, with similar accuracy and efficiency. For the reflection method, the method using the prime function, and the modified series method, a separate $m \times m$ linear system must be solved for the circulations to satisfy the Kutta conditions at the trailing edges of the m airfoils. The velocity potentials for the streaming flow, $w_s(z)$, constant at ∞, and the circulating flows, $w_i(z)$, for flows with unit circulation around each of the m circles for $i = 1, \ldots, m$, must each be computed separately by the three methods. The circulations Γ_i around each circle are then found by solving m equations to satisfy the m Kutta conditions at the images z_j of the trailing edges on the circles,

$$w'(z_j) = w_s'(z_j) + \sum_{i=1}^{m} \Gamma_i w_i'(z_j) = 0;$$

see also [19].

The new aspect of the approach in the present paper is the inclusion of the Kutta conditions for the circulations in a single linear system for the Laurent coefficients of $w(z)$. The efficient

*Received November 28, 2022. Accepted November 20, 2023. Published online on January 8, 2024. Recommended by M. Donatelli.

†Department of Mathematics, Statistics, and Physics, Wichita State University, Wichita, KS 67260-0033, USA (thomas.delillo@wichita.edu, justin.mears@wichita.edu).

‡Data Analysis Consulting, 9009 W Mall Dr, Everett, WA 98208, USA (sahraei.saman@gmail.com).

ETNA
Kent State University and
Johann Radon Institute (RICAM)

solution of the resulting linear systems by conjugate-gradient-like methods was investigated in [9] for circle domains. The purpose of the present paper is to apply that series method for circle domains to compute potential flows in multiply-connected target domains, including multi-element airfoils or smooth domains like those in Figure 1.1. A similar approach to potential flow problems was developed in [18], where the systems are solved by a Gauss-Seidel iteration; see also [21].

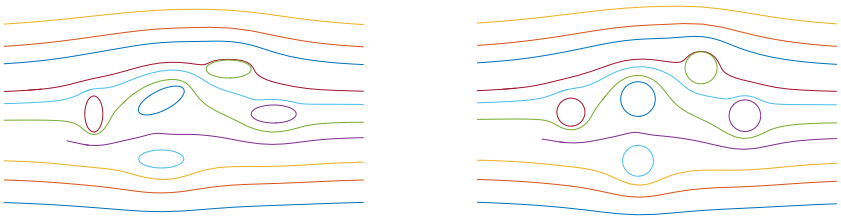

FIG. 1.1. *Potential flow over $m = 5$ smooth boundaries with $N = 128$. The flow is uniform at ∞ with $U = 1$ and the circulations are given around the circles. The (physical) target boundaries are given and the conformal mapping method computes the Laurent series $f(z)$ for the map and the centers and radii of the (unique) conformally equivalent circles (right), where the exterior mapping function is normalized so that $f(z) \sim z$ as $z \to \infty$.*

Numerical methods for computing conformal maps between domains in the complex plane exterior to disks, and domains exterior to airfoils, were used in the past to compute potential flow over single and multi-elements airfoils; see, e.g., Halsey [13] and references in [11]. Here, we perform similar calculations using more recently developed methods for conformal mapping of multiply connected domains [5] with smooth boundaries. We use an extension [5] to exterior multiply connected domains of Fornberg's original method [12], for mapping the unit disk to a simply connected domain bounded by a smooth (continuously turning tangent) curve; see also [10]. Computing the conformal map from the circle domain to the target (physical) domain is a nonlinear problem. The method [12] is a Newton-like method and converges more rapidly than the linearly convergent methods of successive approximation, such as those of Theodorsen and Timman/James; see [15]. Halsey and others [13] used the simply connected exterior method of Timman/James and applied Koebe's method [15, Section 17.7] to successively map domains to the exterior of a disk. More recently developed conformal mapping methods for multiply connected domains [5, 18, 21] produce the map directly to the domain. For airfoils, we successively apply explicit Karman-Trefftz maps to smooth the corners, as described below.

Both the potential flow problem [9] and the conformal mapping method [5] solve linear boundary value problems on the multiply connected circle domains using sums of Laurent series centered on the disks. Discretization is based on N-point trigonometric interpolation on each circle. The linear systems for the conformal maps are inner linear systems arising at each Newton step. These linear systems are solved for the Laurent coefficients and auxiliary parameters such as circulations or conformal moduli (circle centers and radii). An important common feature of both linear systems is that their basic structure is of the form identity plus a low-rank matrix. This means that conjugate gradient methods converge rapidly; see [4] for some related observations.

For introductions to numerical conformal mapping, including methods which map from the physical domain to the computational domain which we do not consider here, see [15, 21]. For introductions to fluid mechanics, see [2, 6], and for applications of complex variables to flow in the plane, see, e.g., [17, 18].

ETNA
Kent State University and
Johann Radon Institute (RICAM)

The paper is organized as follows: Section 2 describes the numerical conformal mapping methods of multiply connected domains exterior to closed curves. Section 3 reviews the series method from [9] for computing potential flow in domains bounded by circles. Linear systems for the Laurent coefficients are solved where the circulations can either be specified, or solved for to satisfy the Kutta condition. Section 4 reports numerical experiments combining the mapping and potential flow methods to compute flow over domains with smooth boundaries and over multi-element airfoils, including examples from [19] and [22]. Section 5 discusses the accuracy of the method. Section 6 states some conclusions and plans for future work.

2. Conformal maps. We give a brief review of the conformal maps used in these calculations following [3, 11].

2.1. Fornberg's method for mapping the exterior of a single smooth closed curve. For completeness, we briefly recall the exterior, simply-connected maps, $m = 1$, although their application will not be discussed here. Details for the numerical method are given in [10] following [12]. For flow over a single airfoil or disk, the series method here and the reflection method in [11] for computing the flow are, of course, identical.

For $m = 1$, the function $\zeta = f(z)$ maps the exterior of the unit disk conformally to the exterior of a smooth, closed curve, $\partial\Omega : \gamma(S)$ with $\gamma'(S)$ continuous. The form of the map is

$$f(z) = a_1 z + a_0 + \sum_{j=1}^{\infty} a_{-j} z^{-j}.$$

Existence and uniqueness of the mapping function is given by the Riemann Mapping Theorem. The numerical method for approximating the (truncated) series for $f(z)$ is a Newton-like method for finding the boundary correspondence $S = S(\theta)$, such that

$$f(e^{i\theta}) = \gamma(S(\theta)).$$

If $S^{(k)}(\theta)$ is the approximation to $S(\theta)$ at the kth Newton step, a correction $U^{(k)}(\theta)$ is computed, such that the boundary values of the linearization,

$$\gamma(S^{(k)}(\theta) + U^{(k)}(\theta)) \approx \gamma(S^{(k)}(\theta)) + \gamma'(S^{(k)}(\theta))U^{(k)}(\theta),$$

are boundary values of a function analytic in the exterior of the disk with a simple pole at ∞. The map is normalized by fixing a boundary point, $f(1) = \gamma(S(0)) = \gamma_0$. The condition for the analytic extension of a function defined on the disk to the exterior of the disk is that the positive indexed Fourier coefficients, $a_j = 0, j = 2, 3, \ldots$. Truncating this condition using N-point trigonometric interpolation, leads to a symmetric positive (semi)definite linear system for $U^{(k)}$, which can be solved efficiently by the conjugate gradient method using the N-point fast Fourier trasform (`fft`). The matrix-vector multiplications therefore cost $O(N \log N)$. The Newton update is

$$S^{(k+1)}(\theta) = S^{(k)}(\theta) + U^{(k)}(\theta),$$

with $U^{(k)}(0) = 0$ to ensure $f(1) = \gamma_0$.

The extension of this approach to the case $m > 1$ [5] is outlined next, following [3, 11]. One difference is worth noting, since it affects the potential flow calculations: for the $m > 1$ case, the map below is normalized by $f(z) = z + O(1/z), z \to \infty$, and the centers and radii of the conformally equivalent circle domain must be computed as part of the problem. The map then satisfies $f'(\infty) = 1$. This condition could be imposed on the $m = 1$ case, and then we would have $a_1 = 1, a_0 = 0$ and the center and radius of the mapped circle would have to be computed, since it would no longer be fixed as the unit circle, in general.

ETNA
Kent State University and
Johann Radon Institute (RICAM)

2.2. Extension of Fornberg's method to exterior multiply connected domains. Existence and uniqueness for the conformal map $\zeta = f(z)$ from the complement, D, of m nonintersecting disks, D_k, in the z-plane, onto a region Ω in the complex ζ-plane which is exterior to m nonintersecting smooth Jordan curves, $\partial\Omega_k$, $1 \le k \le m$, is given in [15, Section 17.1b]. Given Ω and the normalization $f(z) = z + O(1/z)$, $z \approx \infty$, *the circle domain D and the map f are uniquely determined.* Here we give a brief review of the extension [5] of Fornberg's method for computing an approximation to the Laurent series of this map. Boundaries of disks D_k are the circles $C_k : c_k(\theta) := c_k + r_k e^{i\theta}$ and $C = C_1 + \cdots + C_m$. The target boundary of Ω is $\partial\Omega = \partial\Omega_1 + \cdots + \partial\Omega_m$, where the $\partial\Omega_k$ are (smooth) curves parametrized by S, e.g., arclength, $\partial\Omega_k : \gamma_k(S)$. The function f extends smoothly to the boundary $f(C_k) = \partial\Omega_k$. To compute the map, we must find the boundary correspondences $S = S_k(\theta)$ and conformal moduli c_k, r_k, such that

$$f(c_k + r_k e^{i\theta}) = \gamma_k(S_k(\theta)), \quad 1 \le k \le m,$$

where f is analytic and $f(z) = z + O(1/z)$, $z \approx \infty$. Therefore,

$$f(z) = z + \sum_{k=1}^{m} \sum_{k=j}^{\infty} a_{k,j} \left(\frac{r_k}{z - c_k} \right)^j.$$

In place of the condition $a_j = 0, j = 2, 3, \ldots$, for the exterior simply connected map, we use relations among the $a_{k,j}$'s developed in [5] to ensure that a function defined on the boundary extends analytically into the domain D. These conditions are given in the following theorem.

THEOREM 2.1. *Suppose $f \in Lip(C)$ has the Fourier series representation*

$$f(c_k + r_k e^{i\theta}) = \sum_{j=-\infty}^{\infty} a_{k,j} e^{ij\theta}, \quad 1 \le k \le m.$$

Then, f extends analytically into D with $f(z) = z + O(1/z)$ for $z \approx \infty$ if and only if

$$a_{k,j} - \left(\frac{r_k}{c_l - c_k} \right)^j \sum_{l \ne k} \sum_{\nu=0}^{\infty} B_{j+1,\nu} \left(\frac{r_l}{c_k - c_l} \right)^{\nu+1} a_{l,-\nu-1} = r_{k,j}, \quad j \ge 0,$$

where $r_{k,0} = c_k$, $r_{k,1} = r_k$, $r_{k,j} = 0$, for $j \ge 2$, and $B_{k,j}$ denote the binomial coefficients.

Note that for $m = 1$ the conditions would reduce to $a_j := a_{1,j} = 0$, $j \ge 2$. As in the simply connected case, we will linearize the problem about the current guesses for the boundary correspondences, centers and radii, and use a Newton-like iteration. For an initial guess $S_k(\theta)$ and 2π periodic correction $U_k(\theta)$, we use the following linearization for $U_k(\theta)$

$$\gamma_k(S_k(\theta) + U_k(\theta)) \approx \gamma_k(S_k(\theta)) + \gamma_k'(S_k(\theta)) U_k(\theta).$$

For an initial guess of c_k and r_k with corrections δc_k and δr_k,

$$(f + \delta f)(c_k + \delta c_k + (r_k + \delta r_k)e^{i\theta}) \approx (f + \delta f)(c_k + r_k e^{i\theta}) + f'(c_k + r_k e^{i\theta})(\delta c_k + \delta r_k e^{i\theta}).$$

Combining the above approximations gives

$$(f + \delta f)(c_k + r_k e^{i\theta}) = \gamma_k(S_k(\theta)) + \gamma_k'(S_k(\theta)) U_k(\theta) - f'(c_k + r_k e^{i\theta})(\delta c_k + \delta r_k e^{i\theta}).$$

We use the theorem above to force the functions to be boundary values of a function analytic in D. The conditions on the $a_{k,j}$'s are truncated and discretized at N Fourier points on each

ETNA
Kent State University and
Johann Radon Institute (RICAM)

circle. This leads to a linear system for the unknown Newton updates U_k, δc_k, δr_k, denoted by $\underline{U}$, of the form,

$$A\underline{U} = \underline{b},$$

where A is a symmetric positive definite matrix of the form identity plus an effectively low-rank matrix with geometrically decaying singular values. The details are given in [5]. The eigenvalues of A are well-grouped around 1, as is the case for the potential flow equations, below. The system can therefore be solved efficiently by the conjugate gradient method, as in the simply connected case, except that the matrix-vector multiplication now costs $O((mN)^2)$ operations instead of $O(N \log N)$ for the simply connected case. For very high connectivity $O(mN)$ fast multipole methods could be considered for solving the linear systems for both the conformal maps and the potential flow calculations, below. Also, varying N adaptively for close-to-touching boundaries, or boundaries of varying complexity, could be done, if necessary, but such complications are not considered here for the test domains.

The $i+1$st Newton updates are, for $k = 1, \ldots, m$,

$$\begin{aligned} S_k^{i+1} &= S_k^i + U_k^i, \\ c_k^{i+1} &= c_k^i + \delta c_k^i, \\ r_k^{i+1} &= r_k^i + \delta r_k^i. \end{aligned}$$

2.3. Parametrizing the boundary. The Karman-Trefftz maps are constructed by successively conformally transforming a large, finite set of given points along the boundary. The resulting curve must be parametrized by a smooth function with continuously turning tangent (no corners) in order to apply Fornberg's method. We fit the points by two periodic cubic splines for the x and y coordinates parametrized by the chordal arclength, $s_k = \sqrt{(x_{k+1} - x_k)^2 + (y_{k+1} - y_k)^2}$, between two successive points $(x_k, y_k), k = 1, \ldots, N_s$ along the boundary, with $x_{N_s+1} = x_1, y_{N_s+1} = y_1$, based on [16]. This parametrization generally avoids introducing large oscillations into the interpolant, $\gamma(S) = x(S) + iy(S)$, since large changes in the x_k's or y_k's give large changes in the s_k's. For smooth boundaries, such as ellipses in our examples, an analytic parametrization can be used. In such cases, the map extends analytically across the boundary and the map coefficients decay geometrically resulting in spectral accuracy of the truncated series. Fitting the analytic curves with cubic splines reduces the accuracy somewhat, but not dramatically for well-separated, smooth domains, so we use spline fits in all examples here. This approach is probably more realistic in practice where analytic formulas for boundaries may not be available.

2.4. The Karman-Trefftz transformation for airfoils. A classical method for removing a single corner at z_1 on a closed boundary curve of a domain exterior to the curve is the Karman-Trefftz transformation. This has often been used for computing potential flow over the exterior of a multi-element airfoil [13]. The map for a single Joukowski airfoil is illustrated in [11]. The exterior angle $\beta\pi$ at z_1 is smoothed by the Karman-Trefftz transformation, $\zeta = k(z)$, given by

$$\frac{\zeta - \zeta_1}{\zeta - \zeta_2} = \left(\frac{z - z_1}{z - z_2} \right)^{1/\beta},$$

where z_1, the corner, maps to ζ_1 and z_2, a point interior to the the curve, maps to ζ_2. Then,

$$\zeta = k(z) = \left(\zeta_1 - \zeta_2 \left(\frac{z - z_1}{z - z_2} \right)^{1/\beta} \right) \Big/ \left(1 - \left(\frac{z - z_1}{z - z_2} \right)^{1/\beta} \right).$$

ETNA
Kent State University and
Johann Radon Institute (RICAM)

If z_2 is near the leading edge, the map results in a nearly circular set of points which we fit with our periodic cubic spline routine described above. In general, as pointed out in [13], a tracking procedure must be used to ensure that the arguments of the fractional powers vary continuously around the boundary curves.

For the multiply connected case, the Karman-Trefftz transformations are applied successively to the images of the m airfoils to produce a map $k = k_m \circ \cdots \circ k_2 \circ k_1$ from the domain Ω bounded by the airfoils to the domain bounded by nearly circular, smooth curves. Note that each map k_i for the simply connected domain exterior to $\partial\Omega_i$ must be applied to all of the curves at each step. Fornberg's method for exterior multiply connected domains [5] can then be used to compute a Laurent series map $\zeta = h(z)$ from a conformally equivalent domain exterior to m disks to $k(\Omega)$, as described below. The Karman-Trefftz maps k_i can be explicitly inverted,

$$k^{-1}(\zeta) = \left(z_1 - z_2 \left(\frac{\zeta - \zeta_1}{\zeta - \zeta_2} \right)^{\beta} \right) \Big/ \left(1 - \left(\frac{\zeta - \zeta_1}{\zeta - \zeta_2} \right)^{\beta} \right).$$

The final conformal map f from the circle domain to the domain exterior to the m airfoils can be represented as a composition,

$$f = k^{-1} \circ h = k_1^{-1} \circ k_2^{-1} \circ \cdots \circ k_m^{-1} \circ h.$$

3. Complex velocity potential for flow over m cylinders. We briefly review the material in [9]. We want to find the complex velocity potential, $w(z) = \phi(x, y) + i\psi(x, y)$, $z = x + iy$, for ideal, incompressible, irrotational flow in the exterior of m disks such that the velocity is given by $u = \phi_x = \psi_y, v = \phi_y = -\psi_x$, or

$$u - iv = \phi_x - i\phi_y = \phi_x + i\psi_x = w'(z),$$

where $w(z)$ is analytic and the circular boundaries $C_j : z = c_j + r_j e^{i\theta}$ are streamlines, that is, $\psi =$ constant on the C_j's.

The velocity potential can be used to calculate some fundamental quantities for flow around a body with boundary given by a closed curve, C.

THEOREM 3.1. *The circulation Γ of the flow around C and the flux F of the flow through C are given by*

$$\Gamma + iF = \int_C w'(z)dz.$$

Proof. See, e.g., [1, p. 77]. □

We will find the potential flow with circulation, $w(z)$, around multiple disks. The representation of the flow around multiple disks needs to satisfy the following conditions:

1. the C_k's are streamlines, i.e., Im[$w(z)$] = constant for all $z \in C_k,\ k = 1, \ldots, m$;
2. $\lim_{z\to\infty} w'(z) \to U$, uniform flow at ∞;
3. the circulations Γ_k around C_k are either (i) given for $k = 1, \ldots, m$ or (ii) solved for to satisfy the Kutta condition for airfoils.

We use a series representation of the complex velocity potential,

$$w(z) = Uz + \sum_{k=1}^{m} \frac{i\Gamma_k}{2\pi} \ln(z - c_k) + \sum_{k=1}^{m} \sum_{j=1}^{\infty} \left(\frac{r_k}{z - c_k} \right)^j a_{kj}.$$

ETNA
Kent State University and
Johann Radon Institute (RICAM)

The conditions 2 and 3 are satisfied by this expression. We express the condition 1 as $\partial(\operatorname{Im} w(c_k + r_k e^{i\theta})/\partial\theta = 0$ and use the complex velocities,

$$u - iv = w'(z) = U + \sum_{k=1}^{m} \frac{i\Gamma_k}{2\pi r_k} \frac{r_k}{z - c_k} - \sum_{k=1}^{m}\sum_{j=1}^{\infty} \left(\frac{r_k}{z - c_k}\right)^{j+1} j a_{kj}/r_k,$$

to form our linear systems.

3.1. Linear system for the complex velocity potential. We discretize at Fourier points, $z = c_k + r_k e^{\theta_n}, \theta_n = 2\pi n/N, n = 0, \ldots, N-1$, and solve a truncated *linear system* for the a_{kj}'s and (in the case (ii)) for the *circulations* Γ_k*'s* using velocities

$$u - iv = w'(z) = U + \sum_{k=1}^{m} \frac{i\Gamma_k}{2\pi r_k} \frac{r_k}{z - c_k} - \sum_{k=1}^{m}\sum_{j=1}^{J} \left(\frac{r_k}{z - c_k}\right)^{j+1} j a_{kj}/r_k,$$

($J \approx N/2$), satisfying *boundary conditions* above in the form,

1. $\partial(\operatorname{Im} w(c_k + r_k e^{i\theta})/\partial\theta = 0$ for all $z \in C_k$, $k = 1, \ldots, m$;
2. uniform flow at ∞: $\lim_{z\to\infty} w'(z) \to U$;
3. for the *Kutta condition*, the velocities $u(z_k) + iv(z_k) = \overline{w'(z_k)} = 0$ at images of the trailing edges, z_k, determine *circulations* Γ_k around C_k, $k = 1, \ldots, m$.

3.2. Block structure of the real system. Discretizing at the Fourier points, truncating the series to $J = N/2$ terms, using $|U|$, Γ_k real, and taking real parts, we obtain systems in block form.

For the case (i), we have, with $b_{kj} := j a_{kj}/r_k$,

$$\operatorname{Re}\left[\sum_{k=1}^{m}\sum_{j=1}^{J} e^{-i\theta_n} \left(\frac{r_k}{c_l - c_k + r_l e^{-i\theta_n}}\right)^{j+1} b_{kj}\right] = \operatorname{Re}\left[U e^{-i\theta_n}\right] - \sum_{k=1}^{m} \operatorname{Im}\left[\frac{e^{-i\theta_n}/2\pi}{c_l - c_k + r_l e^{-i\theta_n}}\right] \Gamma_k,$$

when the Γ_k's are given. In block matrix form, this can be written as

$$\operatorname{Re}\{A\underline{b}\} = \underline{r} - \operatorname{Im}\{L\}\underline{\Gamma},$$

where $\underline{r}$ is a vector containing the $\operatorname{Re}\left[U e^{-i\theta_n}\right]$'s, $\underline{b}$ is a vector containing the b_{kj}'s, and $\Gamma = [\Gamma_1, \ldots, \Gamma_m]^T$. Separating real and imaginary parts gives

$$\operatorname{Re}\{A\underline{b}\} = [A_R \ -A_I] \begin{bmatrix} b_R \\ b_I \end{bmatrix} = \underline{r} - L_I\underline{\Gamma},$$

where $L_I = \operatorname{Im} L$,

$$L = \begin{bmatrix} L_1 \\ \vdots \\ L_m \end{bmatrix}$$

is an $Nm \times m$ matrix, and L_l is the $N \times m$ submatrix for l fixed.

ETNA
Kent State University and
Johann Radon Institute (RICAM)

For the case (ii), we add m equations for the Kutta condition. We want to solve for the circulations, Γ_l, so that the velocities at the given stagnation points, $z_l = c_l + r_l e^{i\phi_l}$, $l = 1, \ldots, m$, are zero,

$$w'(z_l) = U + \sum_{k=1}^{m} \frac{i\Gamma_k}{2\pi(z_l - c_k)} - \sum_{k=1}^{m}\sum_{j=1}^{\infty} \left(\frac{r_k}{z_l - c_k}\right)^{j+1} b_{kj} = 0.$$

Therefore, we add the following $l = 1, \ldots, m$ (complex) equations for the b_{kj}'s, Γ_k's, to the system,

$$-\sum_{k=1}^{m}\sum_{j=1}^{J} \left(\frac{r_k}{c_l - c_k + r_l e^{i\phi_l}}\right)^{j+1} b_{kj} + \sum_{k=1}^{m} \frac{i}{2\pi(c_l - c_k + r_l e^{i\phi_l})}\Gamma_k = -U.$$

Using $U = |U|e^{-i\alpha}$, multiplying by $e^{i\alpha}$, and using real Γ_i's, we take the imaginary part and add the resulting equations to the other conditions. This leads to a block system,

$$A_S \underline{b}_\Gamma = \left[\begin{array}{ccc} A_R & -A_I & L_I \\ B_I & B_R & C_I \end{array}\right] \left[\begin{array}{c} b_R \\ b_I \\ \hline \Gamma \end{array}\right] = \left[\begin{array}{c} \underline{r} \\ \underline{0} \end{array}\right].$$

where A_R, A_I are $mN \times mJ$ matrices, B_I, B_R are $m \times mJ$, L_I is $mN \times m$, $\Gamma = [\Gamma_1, \ldots, \Gamma_m]^T$, b_R, b_I contain real and imaginary parts of the b_{kj}'s, the vector of unknowns $\underline{b}_\Gamma^T := [b_R^T \;\; b_I^T \;\; \Gamma^T]$, and $\underline{r}_k = [\mathrm{Re}[Ue^{-i\theta_0}], \ldots, \mathrm{Re}[Ue^{-i\theta_{N-1}}]]^T$.

We solve the system (ii) with `cgls` (conjugate gradient for least squares) from [14]. Since the singular values of A_S are well-grouped, `cgls` converges rapidly, as shown in Figure 3.1. The solution for the case (i) where the Γ_k's are given is similar.

3.3. Remark on the Kutta condition. The velocity V is represented as

$$V = V_{\text{stream}} + \Gamma_1 V_1 + \Gamma_2 V_2 + \cdots + \Gamma_m V_m,$$

where V_i is the circulating velocity with circulation 1 around circle C_i and 0 on $C_j, j \neq i$, and V_{stream} is the uniform streaming flow with velocity U at infinity and the circles C_j as streamlines. The Kutta condition selects the unique physical solution by requiring that the velocities at trailing edges are zero. This is achieved by finding the Γ_i's such that

$$V_{\text{stream}}(z_l) + \Gamma_1 V_1(z_l) + \cdots + \Gamma_m V_m(z_l) = 0$$

for $l = 1, \ldots, m$, where the z_l's are the images of the trailing edges on the circles; see [19, eq. 13]. That is, we solve the complex linear system,

$$\left[\begin{array}{ccc} V_1(z_1) & \cdots & V_m(z_1) \\ \vdots & & \vdots \\ V_1(z_m) & \ldots & V_m(z_m) \end{array}\right] \left[\begin{array}{c} \Gamma_1 \\ \vdots \\ \Gamma_m \end{array}\right] = - \left[\begin{array}{c} V_{\text{stream}}(z_1) \\ \vdots \\ V_{\text{stream}}(z_m) \end{array}\right]$$

for real circulations, Γ_i. For our series solutions, above, the imaginary part of the system is incorporated into the full system and solved. A similar approach is used in [18]. The following theorem justifies the assumption that the Γ_i's are real.

THEOREM 3.2. *The complex system above for the circulations satisfying the Kutta condition has a unique, real solution.*

Proof. For a given image z_l of a trailing edge the velocities $V_{\text{stream}}(z_l)$ and $V_k(z_l)$ all have the same direction, since the circles are streamlines, i.e., $V_k(z_l) = r_k e^{i\theta_l}$. Therefore, the complex system can be made real by multiplying each row l by $e^{-i\theta_l}$. ∎

ETNA
Kent State University and
Johann Radon Institute (RICAM)

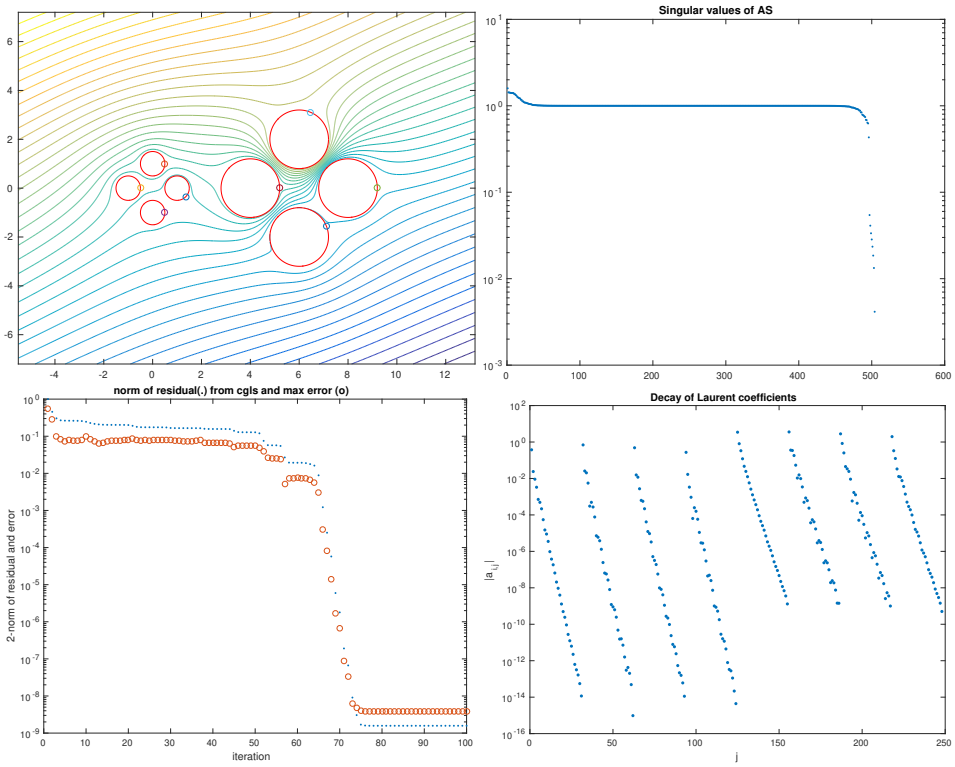

FIG. 3.1. *Flow over $m = 8$ disks using the new combined method solving for the Kutta condition using $N = 64$, $J = 31$ (top left) with singular values (top right), error (bottom left), and decay of coefficients (bottom right). The circulations are computed so that the "o"s on the circles are stagnation points. The streamlines are plotted using the* MATLAB `contour` *function.*

4. Examples of flow calculations. We give a few examples to illustrate the combined methods. First, we give examples of flow over smooth domains where the circulations are given. Some sample timings for various m and N are given in order to compare the relative costs of computing the map and the flow. Next we give some examples of flow over multi-element airfoils, where the circulations Γ_i are computed to satisfy the Kutta condition. Some sample pressure curves over the top and the bottom of the airfoils are also computed.

4.1. Flow over multiply connected smooth domains. In Figure 4.1, the map from the circle domain to the exterior of smooth curves is computed. The circulations can be specified arbitrarily. The level of accuracy is indicated by the decay of the log of the magnitude of the Laurent coefficients: $J = N/2$ for the potential flow and the last $N/2$ coefficients for the conformal map around each circle. The plots illustrate the spectral accuracy of the method for smooth curves.

Some typical sample timings for the map and the flow over smooth regions in Figure 4.2 are given in Table 4.1 for connectivities $m = 2, 4, 8$, computed in MATLAB on a laptop. For the conformal map the number of Newton iterations are fixed at 10 and the number of conjugate gradient iterations are fixed at 30. For the potential flows (with circulations given) we fix the number of `cgls` iterations at 20, resulting in an accuracy of about 10^{-14} in all cases. The dominant operation count is the $O((mN)^2)$ matrix-vector multiplication for solving the conjugate gradient solutions. For large values of N, the fill-in of large matrices begins to dominate the calculations and demands for a more efficient implementation. Timings are

ETNA
Kent State University and
Johann Radon Institute (RICAM)

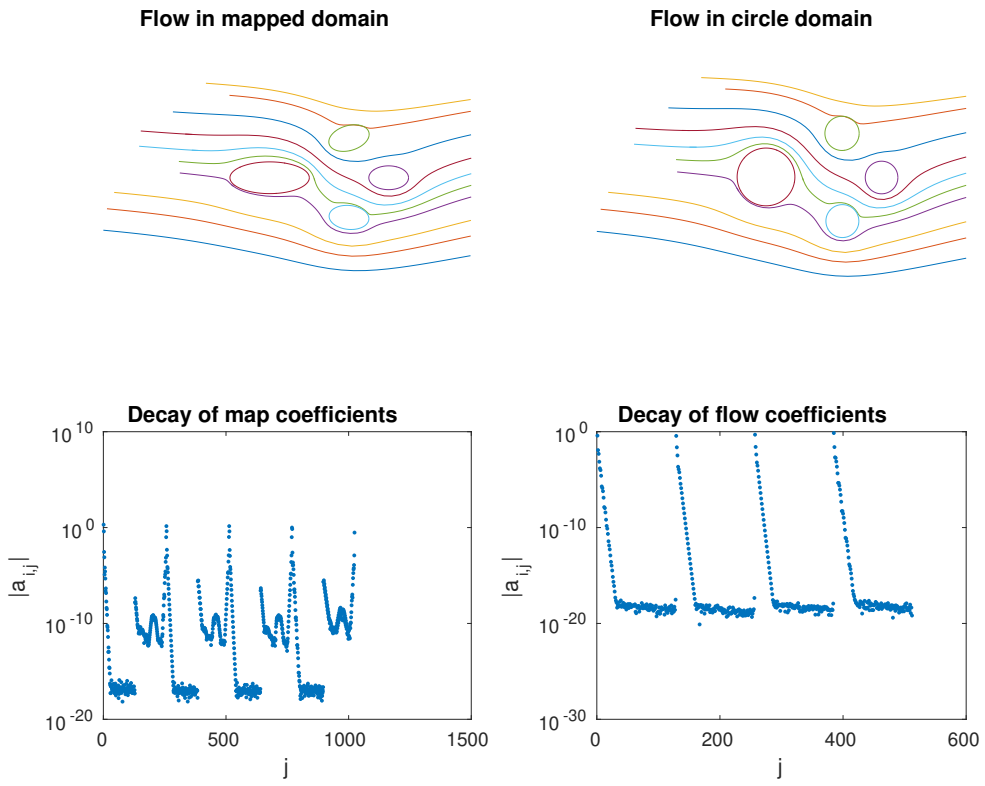

FIG. 4.1. *Potential flow over $m = 4$ smooth boundaries with $N = 256$. The circulations are given as 2 around the three smaller circles and -2 around the large circle.*

similar for airfoils, where the circulations and the preliminary Karman-Trefftz maps have to be computed.

TABLE 4.1
Sample timings in seconds for domains in Figure 4.2.

	$m = 2$		$m = 4$		$m = 8$	
N	map	flow	map	flow	map	flow
64	0.07	0.54	0.20	0.82	0.58	1.95
128	0.15	0.82	0.49	1.86	1.98	6.55
256	0.50	1.44	2.05	4.60	7.96	20.09
512	2.54	4.67	9.69	19.98	79.23	101.97
1024	38.19	22.23	104.69	105.71	603.35	601.68

4.2. Flow over multi-element airfoils. In this setup, the classical Karman-Trefftz transformation k_i, described above, is used to smooth the trailing edge corners successively from each of the m airfoils $\partial\Omega_i, i = 1, \ldots, m$, producing a multiply connected domain with nearly circular, smooth boundaries. The Laurent series method is then used to compute the map h from a domain exterior to non-overlapping disks to the exterior of a domain with smooth

ETNA
Kent State University and
Johann Radon Institute (RICAM)

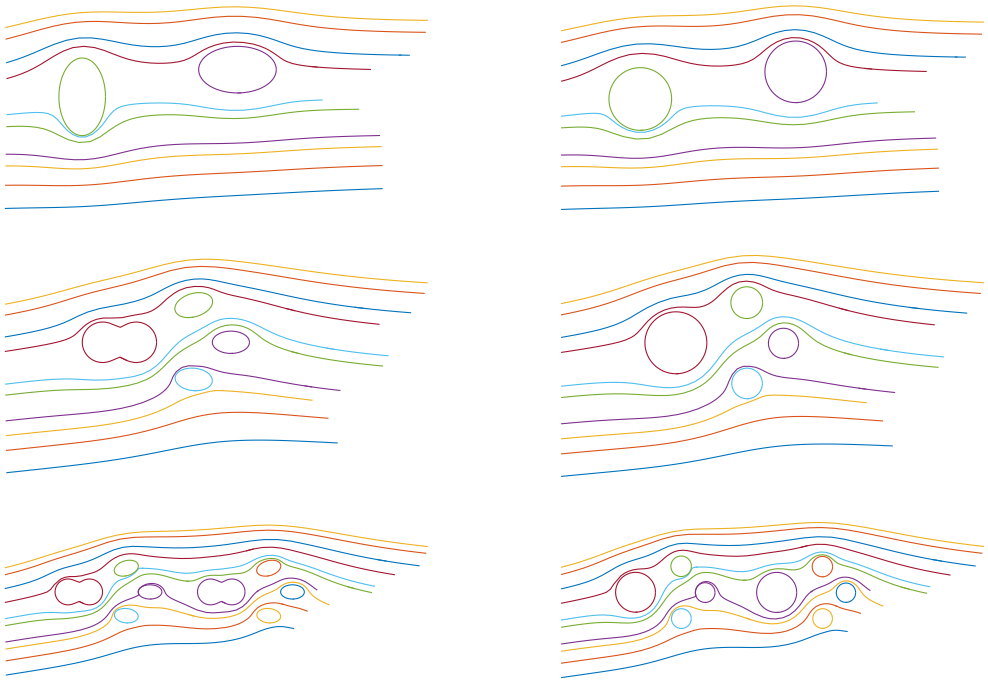

FIG. 4.2. *Potential flow over $m = 2, 4, 8$ smooth boundaries with $N = 64$ for timings in Table 4.1. The circulations are given.*

boundaries. The Karman-Trefftz maps are then inverted to produce a composite map,

$$Z = f(z) = k_1^{-1} \circ k_2^{-1} \circ \cdots \circ k_m^{-1} \circ h(z),$$

from the circle domain to the airfoil domain. The flow is computed in the circle domain by a series method described above, with the circulations calculated to satisfy the Kutta condition, and mapped back to the airfoil domain.

The procedure is illustrated in Figure 4.3 for the map to the exterior of $m = 3$ airfoils (left), where the boundary curves in the middle domain are the result of the application of four successive Karman-Trefftz maps to smooth the trailing edges, and the method [5] is used to compute the map from the exterior of the circles (right) to the exterior of the smooth domain. The X's in the top graph mark the images of the trailing edges, which are calculated on the circles by interpolating the boundary correspondences, so that the Kutta condition can be applied. For this example, we use $m = 3$ cosine curves to define the airfoils,

$$\gamma(\sigma) = -\cos(K\sigma)e^{i\sigma}, \qquad -\frac{\pi}{2K} \le \sigma \le \frac{\pi}{2K},$$

with a trailing edge interior angle $\frac{\pi}{K}$ and $K = 4$. Specifically, the exterior angle is then $\beta\pi = 2\pi - \pi/K = 7\pi/4$ and is removed by the Karman-Trefftz transformation, above, with $\delta = 1/\beta = K/(2K-1) = 4/7$. The β's might be varied for each airfoil, but we have not done this in the examples here.

Since $w'(z) = u - iv$, the streamlines are plotted by numerically solving the system

$$\frac{dx}{dt} = u = \mathrm{Re}\{w'(z)\},$$
$$\frac{dy}{dt} = v = -\mathrm{Im}\{w'(z)\},$$

ETNA
Kent State University and
Johann Radon Institute (RICAM)

by the MATLAB solver `ode45`. This allows us to display streamlines originating near the stagnation points at the trailing edges. The streamlines in the circle domain are then mapped to the airfoil domain.

4.3. Calculating pressures. We calculate the pressure p around the boundaries of the airfoils using Bernoulli's law,

$$p = 1 - |V|^2,$$

where V is the velocity. The complex velocity potential $W(Z)$ in the physical (airfoil) Z-plane in terms of the velocity potential $w(z)$ in the circle domain and the conformal map $Z = f(z)$ is given by

$$W(Z) = W(f(z)) = w(z) = w(f^{-1}(Z)).$$

Therefore, V is given by

$$\overline{V} = \frac{dW}{dZ} = \frac{d}{dZ} w(f^{-1}(Z)) = w'(z)\frac{dz}{dZ} = w'(z)/f'(z).$$

For uniform velocity U_Z at ∞ in the physical Z-plane, we need

$$\overline{U}_Z = w'(\infty)/f'(\infty) = \overline{U}/f'(\infty),$$

where U is the uniform velocity in the circle z-plane. Note that, since $f(z) = k^{-1}(h(z))$,

$$f'(z) = (k^{-1})'(h(z))h'(z).$$

The Fornberg map $h(z)$ has $h(\infty) = \infty, h'(\infty) = 1$. For a single inverse Karman-Trefftz map, $k_i^{-1}(\zeta)$, a calculation gives

$$(k_i^{-1})'(\infty) = \frac{1}{\beta}\left(\frac{z_2 - z_1}{\zeta_2 - \zeta_1}\right).$$

Therefore, we need

$$\overline{U} = \overline{U}_Z f'(\infty) = \overline{U}_Z \left(\frac{z_2 - z_1}{\zeta_2 - \zeta_1}\right)/\beta.$$

Pressure curves are displayed for the airfoil examples below.

4.4. A 2-airfoil example from Williams's paper. Figure 4.4 displays flow for configuration A from [22, Table p. 7] with $\alpha = 0$, solving the full combined system above for the Laurent coefficients and the circulations with $N = 128$ and $k_{\text{steps}} = 25$ conjugate gradient iterations. A function for tracking the roots continuously for the Karman-Trefftz maps is used in our examples. Also, the Fornberg map iterations are smoothed by zeroing the 3 highest order Fourier coefficients. Here, the computed circulations for $N = 128$ are 1.3889486... and 0.4773498.... The circulations listed in [22] are 1.3909 and 0.4784. They are calculated from a reflection method for the flows, as in [11], which is generally less accurate than the series method, unless many levels of reflection are used. Also, 2 to 4 digit accuracy is usually all one can expect composing Fourier series conformal mapping methods with methods to smooth corners; see [3]. In practice, airfoil shapes are not defined more accurately, so this is not a serious limitation. The shape and range of the pressure curves obtained here are similar to [22].

ETNA
Kent State University and
Johann Radon Institute (RICAM)

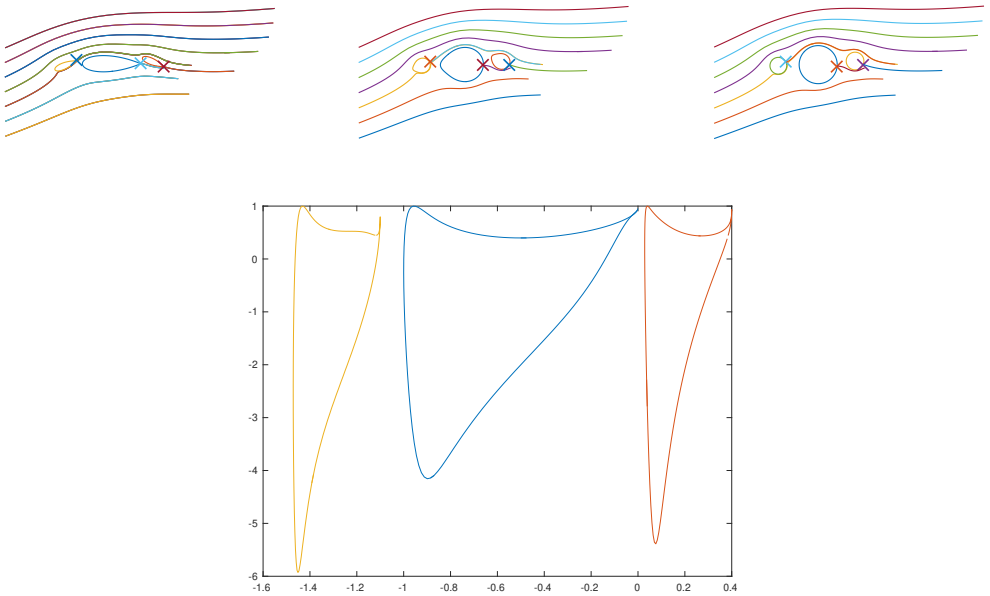

FIG. 4.3. *Conformal map $f = k^{-1} \circ h$, where composition of Karman-Trefftz maps $k = k_1 \circ k_2 \circ k_3$ successively smooth corners (left), Laurent series map h maps from circle domain (right) to smooth domain (center), and potential flow with Kutta condition at trailing edges (X) is computed in circle domain by Laurent series and $N = 128$ Fourier points on each circle with $U = e^{i\pi/16}$, $K = 4$, $N_s = 100$. Pressures on the upper and lower portion of each airfoil are plotted in the lower figure. The horizontal axis is the real part of the points on the airfoil.*

4.5. A 3-airfoil example from Suddhoo and Hall's paper. Figure 4.5 and Table 4.2 show flow results for configuration B from [19], solving the full combined linear system above for the Laurent coefficients and the circulations with $N = 128$. The circulations are 1.46857660, 0.8840742, and 6.4221982. The corresponding circulations listed in [19] are 1.4747, 0.8849, and 6.4355. The increase in accuracy, shown in Table 4.2, of about one decimal place for each doubling of N, illustrates the roughly third-order accuracy due to the spline interpolation used to find the preimages of the trailing edges, as discussed in Section 5. The accuracy ϵ of the boundary conditions, defined in Section 5, is roughly spectral. The pressure curves (bottom graph) are similar to the Figure in [19].

TABLE 4.2
Sample timings (in seconds), circulations, Γ_i, and accuracy of the MATLAB *code on a laptop for an airfoil from [19] for $m = 3$, configuration B, with angle of attack $\alpha = 20^o$; see Figure 4.5 for the conformal map and the full linear systems for the flow, using $k_{steps} = 35$ conjugate gradient (CG) iterations. Operation counts for the flow and the map are $O((mN)^2 \times k_{steps})$.*

N	map	flow	Γ_1	Γ_2	Γ_3	ϵ
32	0.12	0.30	1.46716332	0.8929293	6.4021316	$1.4 \cdot 10^{-04}$
64	0.23	0.34	1.46893074	0.8825023	6.4254065	$1.8 \cdot 10^{-07}$
128	0.77	0.55	1.46857660	0.8840742	6.4221982	$9.9 \cdot 10^{-13}$
256	3.37	1.08	1.46856840	0.8841090	6.4221244	$1.2 \cdot 10^{-14}$

4.6. A 4-airfoil example from Suddhoo and Hall's paper. Flow for configuration A from [19] is an exact test case generated by applying $m = 4$ inverse Karman-Trefftz transformations successively to chosen circles. The exact map from the exterior of 4 disks is

ETNA
Kent State University and
Johann Radon Institute (RICAM)

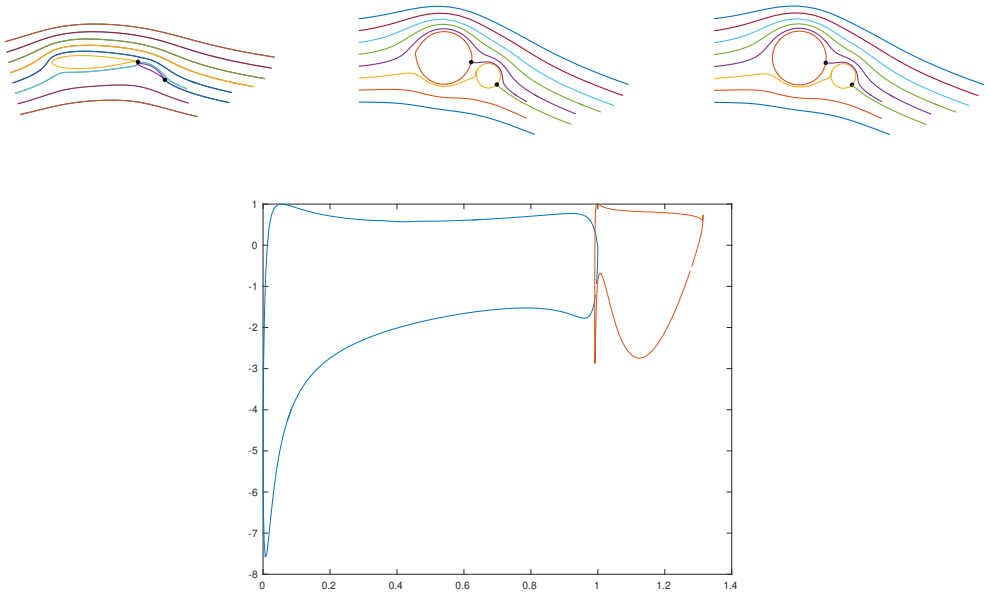

FIG. 4.4. *Flow for configuration A from [22] using the full series with $N = 128$ and angle of attack $\alpha = 0$, and corresponding pressure curves (bottom).*

produced by the sequence of maps shown in Figure 4.6. The map for the 3-airfoil case, above, is produced similarly. A different sequence of Karmann-Trefftz maps, of course, is used to smooth corners and compose with the Laurent series maps for these test cases. The flow for in this case is shown in Figure 4.7. The flow is computed using the series and Fornberg map with $N = 128$ Fourier points and angle of attack $\alpha = 0$. The circulations are 0.521940..., 2.07956..., 0.72166..., and 4.71673.... The corresponding circulations listed in [19] are 0.5215, 2.0794, 0.7216, and 4.7157. Again, 3 or 4 digit accuracy is usually all one can expect; see Table 4.3 for sample timing and accuracy. The pressure curves (bottom graph) are similar to the Figure in [19].

TABLE 4.3
Sample timings (in seconds), circulations, Γ_i, and accuracy of the MATLAB *code on a laptop for an airfoil from [19] for $m = 4$, configuration A, with angle of attack $\alpha = 0$; see Figure 4.7 for the conformal map and the full linear systems for the flow, using $k_{steps} = 40$ CG iterations. Operation counts for the flow and the map are $O((mN)^2 \times k_{steps})$.*

N	map	flow	Γ_1	Γ_2	Γ_3	Γ_4	ϵ
64	0.37	0.38	0.522048	2.07908	0.72162	4.71769	$1.3 \cdot 10^{-07}$
128	1.39	0.87	0.521940	2.07956	0.72166	4.71673	$4.8 \cdot 10^{-13}$
256	7.16	1.91	0.521939	2.07957	0.72167	4.71672	$7.5 \cdot 10^{-15}$

5. Some comments on convergence and accuracy. The analytic velocity potential $w(z)$ for the flow over m disks exists and is unique if the velocity at infinity is given and the circulations are given or determined by the Kutta condition. Our estimates of accuracy and our analysis of convergence depends on some numerical observations. For $J = N/2$, there are exactly m singular values of A_S with $\sigma_k \approx 10^{-15}$. We generally select $J = N/2 - 1$. Then, these m "zero" singular values are perturbed to about $1 > \sigma_k > 10^{-3}$; see, e.g., Figure 3.1.

ETNA
Kent State University and
Johann Radon Institute (RICAM)

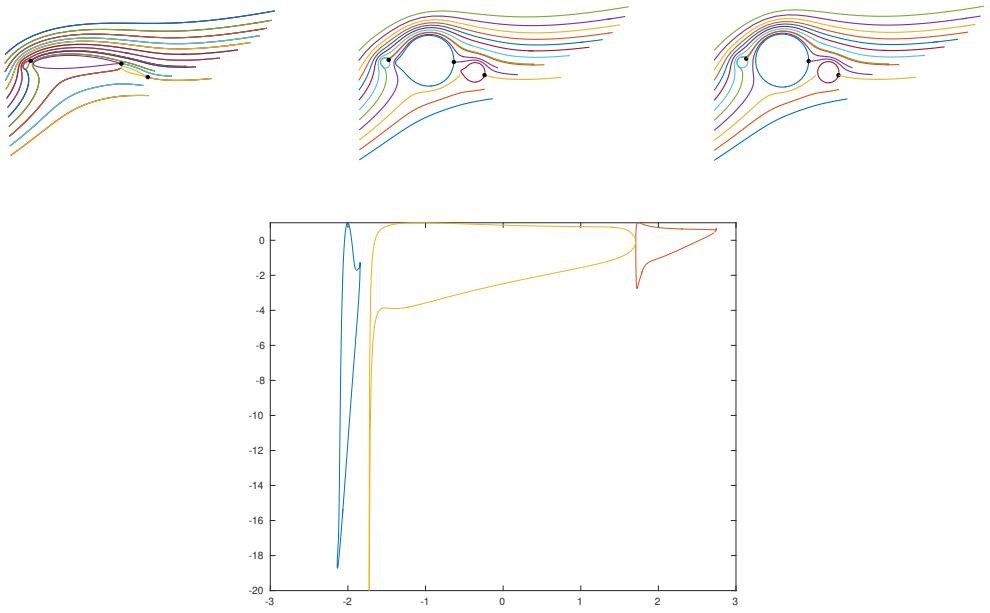

FIG. 4.5. *Flow for configuration B from [19] using the full series with* $N = 128$ *and angle of attack* $\alpha = 20^o$*, and corresponding pressure curves (bottom).*

These values are independent of N and α, and depend mainly on the C_j's. A discussion of these effects for similar systems is given in [4, 9]. Choosing $J < N/2 - 1$ does not generally change these observations. Therefore, with $J = N/2 - 1$ the matrix A_S is full rank and it is possible to prove by standard theorems that conjugate-gradient-like methods converge. The convergence is superlinear due to the fact that the eigenvalues of $A_S^T A_S$ (the squares of the singular values of A_S) are well-grouped around 1, with about $2m$ outliers slightly greater than or less than 1; see Figure 3.1.

One measure ε of the error (used in [9]) is defined by taking the difference of the imaginary parts of the potential $w(z)$ at $2N$ Fourier points, $z_{k,n} = c_k + r_k e^{i\theta_n} \in C_k$, where $\theta_n = 2\pi n/2N$, $n = 0, \ldots, 2N-1$, with the average value at the N Fourier points used to solve the system. Let $\zeta_{k,j} = c_k + r_k e^{it_j}$, $t_j = 2\pi j/\mathrm{N}$, $j = 0, \ldots, N-1$, be the collocation points for our construction of $w(z)$. Then, let

$$\varepsilon_{k,n} := \left| \operatorname{Im}\left[w(z_{k,n})\right] - \frac{1}{N} \sum_{j=0}^{N-1} \operatorname{Im}\left[w(\zeta_{k,j})\right] \right|.$$

The overall error ε is then given by

$$\begin{aligned} \varepsilon_k &:= \max_n \varepsilon_{k,n}, \\ \varepsilon &:= \max_k \varepsilon_k. \end{aligned}$$

This error estimate provides a good measure of how the imaginary parts of the velocity potential are nearly constant on the circles. Convergence of the error ε of the CG iterates to the level of accuracy for the given N takes place superlinearly in $O(2m)$ steps, as expected. As shown by examples in [9], we generally see spectral accuracy, i.e., errors squaring when N is doubled. Overall accuracy may be less when we conformally map to domains with corners, as discussed in [11] and below.

ETNA
Kent State University and
Johann Radon Institute (RICAM)

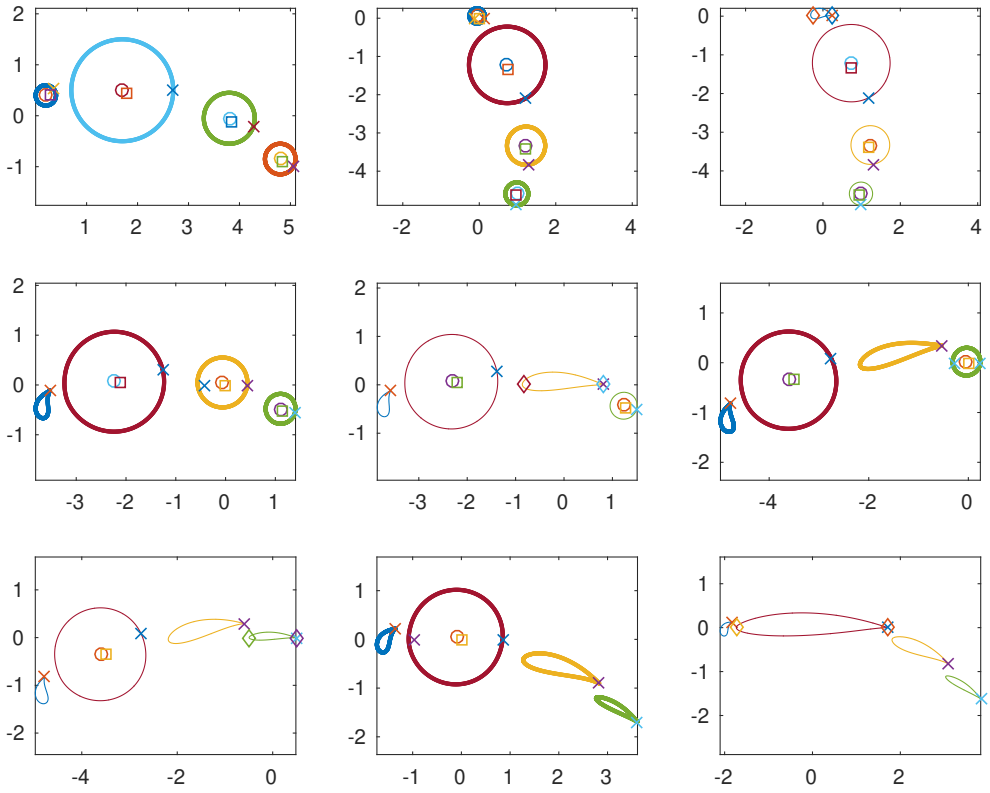

FIG. 4.6. *Sequence of maps for configuration A from [19], an exact test case generated by applying $m = 4$ inverse Karman-Trefftz transformations successively to chosen circles.*

REMARK 5.1. If $J = N/2$ is chosen, the iterations will initially converge and then diverge due to the presence of near-zero singular values. Such semi-convergence is familiar for ill-conditioned systems that occur, for instance, in the solution of inverse problems. Taking $J = N/2 - 1$, or damping higher order coefficients, may therefore be regarded as a form of regularization. Such "smoothing" of higher-order Fourier coefficients has been found to be an effective way of handling semi-convergence of iterates for similar problems in numerical conformal mapping; see, e.g., [21, p. 403].

To discuss convergence of our solutions as $N \to \infty$, we will work with the exact series for $w'(z)$. We will write now this series as

$$w'(z) = b_0 + \sum_{k=1}^{m} \sum_{j=1}^{\infty} \left(\frac{r_k}{z - c_k} \right)^j b_{kj},$$

where now $b_0 := U$, $b_{k1} := i\Gamma_k/2\pi r_k$, and $b_{kj} := -j a_{kj}/r_k$, $j = 2, \ldots, \infty$, $k = 1, \ldots, m$. Since the solution to the potential flow problem for a given circle domain, with U and the Γ_k's given, is unique, this series clearly satisfies our boundary conditions,

$$\operatorname{Im} w'(z) = 0, \quad z \in C_k, \quad k = 1, \ldots, m.$$

Next, note that $w'(z)$ extends analytically across the C_k's up the radius determined by the nearest singularities inside C_k. As discussed in [9], the construction of the solution $w(z)$ by

ETNA
Kent State University and
Johann Radon Institute (RICAM)

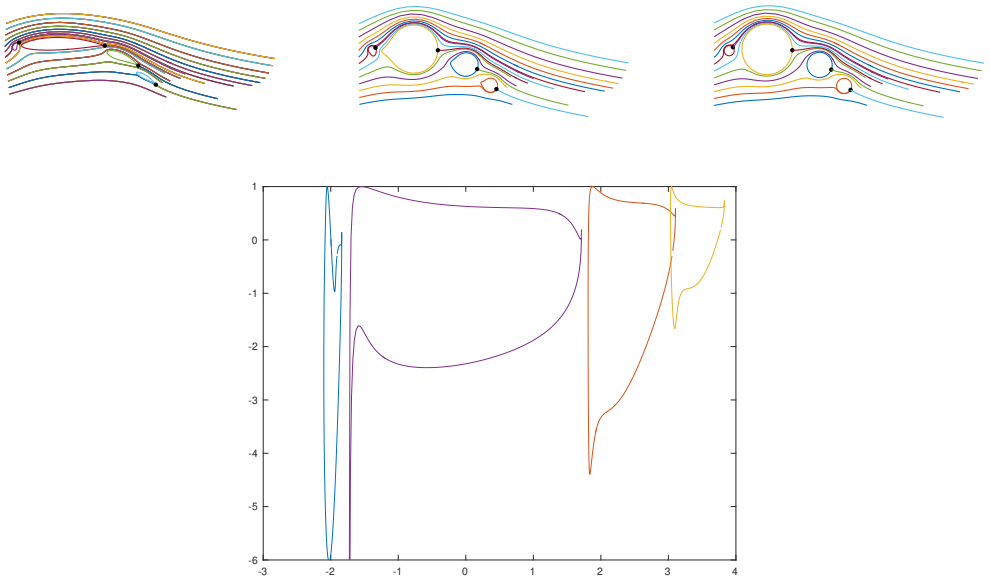

FIG. 4.7. *Flow for configuration A from [19] using the full series with* $N = 128$ *and angle of attack* $\alpha = 0$*, and corresponding pressure curves (bottom).*

the reflection method (method of images) shows that for two circles C_j and C_k the nearest singularity to C_k inside C_j is determined by the limit of the successive reflection of the centers of the two circles. This limit is a fixed point ζ_{kj} of the Moebius map formed by reflection in C_j followed by reflection in C_k. Let

$$R_j = \max_k \frac{|\zeta_{kj} - c_j|}{r_j} < 1.$$

Then, $|a_{ji}| \le CR_j^i$. Taking $R = \max_j R_j < 1$, we have

$$|b_{kj}| \le CjR^j \to 0, \quad j \to \infty, \quad \text{for all } k, j \text{ and some } C > 0.$$

Now, consider the truncated series

$$w'_J(z) = b_0 + \sum_{k=1}^{m} \sum_{j=1}^{J} \left(\frac{r_k}{z - c_k} \right)^j b_{kj}.$$

Then, since $|r_k/(z - c_k)| \le 1$ for $z \in C_j$, $j = 1, \ldots, m$,

$$\text{Im } |w'_J(z)| \le CJR^J \to 0, \quad J \to \infty, \quad \text{for some } C > 0.$$

Therefore, if b denotes the vector of real and imaginary parts of the b_{kj}'s, as above, then b satisfies a linear system, derived as above from discretizing in z at N Fourier points on each circle, of the form,

$$A_S b = r + e.$$

Here r denotes the right-hand side for the discrete system and the error vector e, due to truncating the infinite series, satisfies $\|e\|_\infty = O(JR^J)$. Note from above that A_S is a

ETNA
Kent State University and
Johann Radon Institute (RICAM)

$(Nm+m)\times(2Jm+m)$ matrix of full rank $2Jm+m$ when $J = N/2-1$ in our examples. For a given domain, we have found that the outlying singular values of A_S, σ_1 and $\sigma_{2Jm+m} > 0$ do not change much with N. Therefore, the condition number of A_S, $\kappa(A_S) = \sigma_1/\sigma_{2Jm+m}$, does not grow with N. Let the SVD of A_S be

$$A_S = \sum_{j=1}^{2Jm+m} \sigma_j u_j v_j^T.$$

Now let $\hat{b}$ be the solution to the discrete system from above, now written as

$$A_S\hat{b} = r,$$

for convenience. Then,

$$A_S(b-\hat{b}) = e$$

and therefore

$$\hat{b} = b - \sum_{j=1}^{2Jm+m} v_j \frac{u_j^T e}{\sigma_j}.$$

Since $\|e\|_\infty$ converges to 0 like $O(JR^J)$ as $N \to \infty$, $\hat{b}$ will converge to b. We have therefore proven the following theorem.

THEOREM 5.2. *If the circle domain bounded by given C_j's, $j = 1\ldots,m$, is such that condition numbers of the family of matrices A_S, formed for each N and $J = N/2-1$, remain uniformly bounded, then the approximate velocity potentials will converge to the exact potential $w(z)$ as $N \to \infty$.*

We illustrate the accuracy and convergence with the following two examples.

EXAMPLE 5.3. See Figure 5.1, where we compute the flow over $m = 2$ ellipses. The circulations Γ_1, Γ_2 are given. The errors are listed in Table 5.1. The average values of Im $w(z)$ at $2N$ Fourier points converge roughly quadratically as N is doubled. The error in the conformal map is approximated by how nearly the real and imaginary parts of the map $f(z)$, evaluated at $2N$ Fourier points on the circles, satisfy the equations for the elliptical boundaries. These errors also converge quadratically, as expected for analytic boundaries. We used our periodic cubic spline with a very large number $N_s = 8000$ of knots to fit the ellipse boundaries in the conformal mapping code. The accuracy using the analytic parametrization is similar.

TABLE 5.1
Average values of Im $w(z)$, $z \in C_1, C_2$, for $m = 2$ smooth boundaries and overall accuracy of conformal map in Figure 5.1, $N_s = 8000$, $J = N/2-1$; $\Gamma_1 = \Gamma_2 = 2$ are given, $\sigma_{min}(AS) \approx 0.8$ for all N.

N	Im $w(z), z \in C_1$	Im $w(z), z \in C_2$	map accuracy
16	0.114391338010714	-0.350081754431789	$1.1 \cdot 10^{-02}$
32	0.114295133088431	-0.349692481939068	$5.6 \cdot 10^{-05}$
64	0.114295784168430	-0.349691589528057	$9.1 \cdot 10^{-09}$
128	0.114295784171233	-0.349691589519629	$1.6 \cdot 10^{-14}$
256	0.114295784171233	-0.349691589519634	$1.6 \cdot 10^{-14}$

EXAMPLE 5.4. Here we consider the domain in Figure 4.3 for flow over $m = 3$ airfoils. Errors are given in Table 5.2. In this case the full system is solved for the Laurent coefficients

ETNA
Kent State University and
Johann Radon Institute (RICAM)

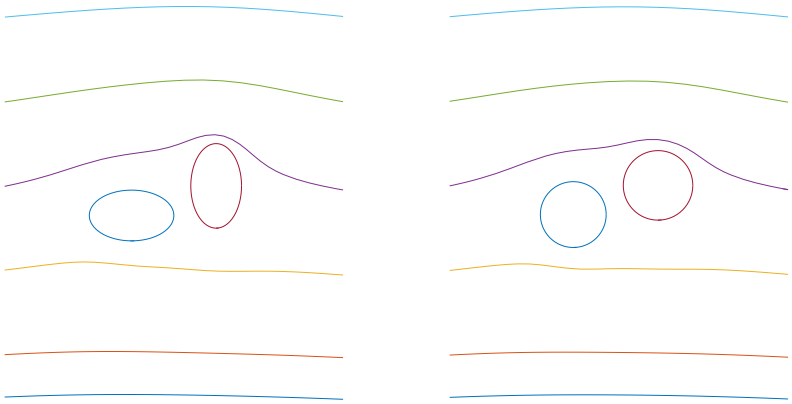

FIG. 5.1. *Streamlines for flow exterior to $m = 2$ ellipses, with $N = 6$, $\Gamma_1 = \Gamma_2 = 2$, and $U = 1$.*

and the circulations satisfying the Kutta condition. The values for the circulation Γ_1, Im $w(z)$ at $2N$ Fourier points, and the argument ϕ_1 of the stagnation point on the middle (largest) circle C_1 are listed. The convergence is much slower here and the accuracy does not improve much beyond about 6 digits. The results for the other two boundaries are similar. The accuracy is limited here by the accuracy of the conformal map. It is difficult to accurately compute the preimages (with arguments ϕ_k) of the trailing edges of the airfoils. These preimages do not generally fall on Fourier points on the circles and their locations have to be computed by interpolation. The inverse of the boundary correspondences $\theta_k = \theta_k(S)$ is approximated by interpolating the mesh points with a cubic spline. Then $\phi_k = \theta_k(0)$ or $\theta_k(2\pi)$, corresponding to the images of the trailing edges on the smooth curves. Accuracy of the interpolation is therefore roughly third order, as can be seen in the tables. In general, it is difficult to compute conformal maps to domains with corners accurately to more than a few digits using Fourier series; see, e.g., [11].

TABLE 5.2
Accuracy of Γ_1, Im $w(z), z \in C_1$, and ϕ_1 for middle circle and overall accuracy ε in Figure 4.3, $m = 3, N_s = 8000, J = N/2 - 1$. The accuracies for C_2 and C_3 are similar; $\sigma_{min}(AS) \approx 10^{-2}$ for all N.

N	Γ_1	Im $w(z), z \in C_1$	ϕ_1	ε
32	1.0958944619	-0.0700282779	6.2698640405	$9.8 \cdot 10^{-07}$
64	1.3914187475	-0.0733887932	6.2113250060	$4.3 \cdot 10^{-11}$
128	1.3905777394	-0.0733406660	6.2102720760	$5.4 \cdot 10^{-16}$
256	1.3905512683	-0.0733404812	6.2102694711	$6.4 \cdot 10^{-16}$
512	1.3906294182	-0.0733411579	6.2102693434	$1.0 \cdot 10^{-15}$
1024	1.3906293929	-0.0733411724	6.2102699099	$3.1 \cdot 10^{-15}$

6. Conclusions and future work. We have presented an efficient method for computing potential flow in the plane using conformal mapping. Our conformal mapping method can also be replaced by Wegmann's similar Newton-like method. Also, Wegmann's [21] version of Prosnak's projection method [18] can be used to map directly to the airfoil domain. The projection method does not require smooth boundaries, but is only linearly convergent. We plan more extensive comparisons of our series method with the method based on the prime function, as in [8]. Interior flows in bounded multiply-connected domains will also be computed. Quantities such as moments and lift coefficients can also be calculated form our potential

ETNA
Kent State University and
Johann Radon Institute (RICAM)

functions, and compared to results in the engineering literature. In addition, it should also be possible to solve efficiently the flow problems directly in the physical domain using series similar to those proposed in [20], thus avoiding computation of the conformal maps. We plan to make comparisons of these alternatives, along with more traditional methods based on integral equations, in future work, but we will not pursue this here. These methods will provide efficient tools for initial designs in preparation for more expensive CFD simulations.

Acknowledgements. This work was partially supported by a grant to the first author from the Simons Foundation and funds from the Alan R. Elcrat Professorship of Applied Mathematics. Some of the work was carried out during a visit to the Isaac Newton Institute, Cambridge, UK, during the first author's sabbatical leave from Wichita State University in Fall 2019. The authors thank the referee for suggestions that improved the paper.

REFERENCES

[1] M. J. Ablowitz and A. S. Fokas, *Complex Variables: Introduction and Applications*, Cambridge University Press, Cambridge, 2003.
[2] D. J. Acheson, *Elementary Fluid Dynamics*, Clarendon Press, Oxford, 1990.
[3] M. Badreddine, T. K. DeLillo and S. Sahraei, *A comparison of some numerical conformal mapping methods for simply and multiply connected domains*, Discret. Contin. Dyn. Syst.-Ser. B, 24 (2019), pp. 55–82.
[4] R. Balu and T. K. DeLillo, *Numerical methods for Riemann-Hilbert problems in multiply connected circle domains*, J. Comput. Appl. Math., 307 (2016), pp. 248–261.
[5] N. Benchama, T. DeLillo, T. Hrycak, and L. Wang, *A simplified Fornberg-like method for the conformal mapping of multiply connected regions–comparisons and crowding*, J. Comput. Appl. Math., 209 (2007), pp. 1–21.
[6] S. Childress, *An Introduction to Theoretical Fluid Mechanics*, Courant Lecture Notes 19, AMS, Providence, 2009.
[7] D. Crowdy, *Solving Problems in Multiply Connected Domains*, CBMS-NSF Regional Conference Series in Applied Mathematics 97, SIAM, Philadelphia, 2020.
[8] T. K. DeLillo and C. C. Green, *Computation of plane potential flow around multi-element airfoils using the Schottky-Klein prime function*, Physica D, 450 (2023), Art. 133753 (14 pages).
[9] T. K. DeLillo, J. Mears, and A. Silva-Trujillo, *Potential flow in a multiply connected circle domain using series methods*, J. Comput. Appl. Math., 391 (2021), Art. 113445 (16 pages).
[10] T. K. DeLillo and J. A. Pfaltzgraff, *Numerical conformal mapping methods for simply and doubly connected regions*, SIAM J. Sci. Comput., 19 (1998), pp. 155–171.
[11] T. K. DeLillo and S. Sahraei, *Computation of plane potential flow past multi-element airfoils using conformal mapping, revisited*, J. Comput. Appl. Math., 362 (2019), pp. 246–261.
[12] B. Fornberg, *A numerical method for conformal mappings*, SIAM J. Sci. Stat. Comput., 1 (1980), pp. 386–400.
[13] N. D. Halsey, *Potential flow analysis of multielement airfoils using conformal mapping*, AIAA J., 17 (1979), pp. 1281–1288.
[14] P.-C. Hansen, *Regularization Tools: A Matlab Package for Analysis and Solution of Discrete Ill-Posed Problems*, version 2.0 for Matlab 4.0 (1992, revised 1998); see Numer. Algor., 6 (1994), pp. 1–35; software available via netlib@research.att.com from directory NUMERALGO.
[15] P. Henrici, *Applied and Computational Complex Analysis, Volume 3: Discrete Fourier Analysis, Cauchy Integrals, Construction of Conformal Maps, Univalent Functions*, Wiley, New York, 1993.
[16] W. D. Hoskins and P. R. King, *Periodic cubic spline interpolation using parametric splines*, Comput. J., 15 (1972), pp. 282–283.
[17] L. M. Milne-Thomson, *Theoretical Aerodynamics*, Dover, New York, 1973.
[18] W. J. Prosnak, *Computation of Fluid Motions in Multiply Connected Domains*, G. Braun, Karlsruhe, 1987.
[19] A. Suddhoo and I. M. Hall, *Test cases for the plane potential flow past a multi-element airfoil*, Aeronaut. J., 89 (1985), pp. 403–414.
[20] L. N. Trefethen, *Series solution of Laplace problems*, Anziam J., 60 (2018), pp. 1–26.
[21] R. Wegmann, *Methods for numerical conformal mapping*, in *Handbook of Complex Analysis, Geometric Function Theory, Vol. 2*, R. Kuehnau, ed., Elsevier, Amsterdam, 2005, pp. 351–477.
[22] B. R. Williams, *An exact test case for the plane potential flow about two adjacent lifting airfoils*, RAE Technical Report No. 3717, London (1973). Available at https://reports.aerade.cranfield.ac.uk/bitstream/handle/1826.2/2993/arc-rm-3717.pdf